ACCOUNTS
of chemical research

Synthesis and Stabilization of Supported Metal Catalysts by Atomic Layer Deposition

JUNLING LU,[†] JEFFREY W. ELAM,[†] AND PETER C. STAIR*,[‡,§]

[†]*Energy Systems Division and* [‡]*Chemical Sciences & Engineering Division, Argonne National Laboratory, Argonne, Illinois 60439, United States, and* [§]*Department of Chemistry, Northwestern University, Evanston, Illinois 60208, United States*

RECEIVED ON JULY 31, 2012

CONSPECTUS

Supported metal nanoparticles are among the most important catalysts for many practical reactions, including petroleum refining, automobile exhaust treatment, and Fischer–Tropsch synthesis. The catalytic performance strongly depends on the size, composition, and structure of the metal nanoparticles, as well as the underlying support. Scientists have used conventional synthesis methods including impregnation, ion exchange, and deposition–precipitation to control and tune these factors, to establish structure–performance relationships, and to develop better catalysts. Meanwhile, chemists have improved the stability of metal nanoparticles against sintering by the application of protective layers, such as polymers and oxides that encapsulate the metal particle. This often leads to decreased catalytic activity due to a lack of precise control over the thickness of the protective layer.

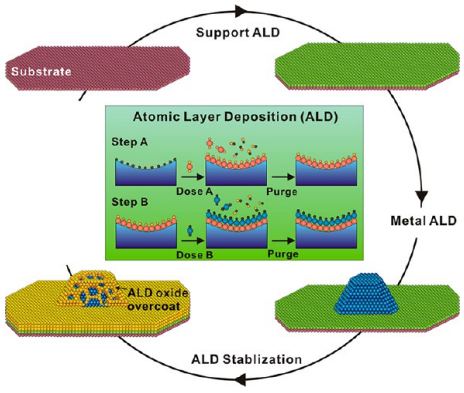

A promising method of catalyst synthesis is atomic layer deposition (ALD). ALD is a variation on chemical vapor deposition in which metals, oxides, and other materials are deposited on surfaces by a sequence of self-limiting reactions. The self-limiting character of these reactions makes it possible to achieve uniform deposits on high-surface-area porous solids. Therefore, design and synthesis of advanced catalysts on the nanoscale becomes possible through precise control over the structure and composition of the underlying support, the catalytic active sites, and the protective layer. In this Account, we describe our advances in the synthesis and stabilization of supported metal catalysts by ALD. After a short introduction to the technique of ALD, we show several strategies for metal catalyst synthesis by ALD that take advantage of its self-limiting feature. Monometallic and bimetallic catalysts with precise control over the metal particle size, composition, and structure were achieved by combining ALD sequences, surface treatments, and deposition temperature control.

Next, we describe ALD oxide overcoats applied with atomically precise thickness control that stabilize metal catalysts while preserving their catalytic function. We also discuss strategies for generation and control over the porosity of the overcoats that allow the embedded metal particles to remain accessible by reactants, and the details for ALD alumina overcoats on metal catalysts. Moreover, using methanol decomposition and oxidative dehydrogenation of ethane as probe reactions, we demonstrate that selectively blocking low coordination metal sites by oxide overcoats can provide another strategy to enhance both the durability and selectivity of metal catalysts.

1. Introduction

Transition-metal nanoparticles on oxide supports are objects of great interest in heterogeneous catalysis due to their unique chemical and physical properties. They are widely used in petroleum refining, automobile exhaust treatment, Fischer–Tropsch synthesis, water gas shift, and many other processes. Substantial effort has been devoted to improving control over the size, composition, and morphology of metal nanoparticles to obtain highly uniform species that are expected to exhibit higher selectivity compared with catalysts that are profoundly inhomogeneous.[1,2] Improving the stability of metal particles against sintering under reaction conditions has also drawn a lot of attention, especially for applications in high temperature reactions, since it is a

Published on the Web 03/12/2013 www.pubs.acs.org/accounts
10.1021/ar300229c

SCHEME 1. General ALD Binary Reaction Sequence for Layer-by-Layer Growth

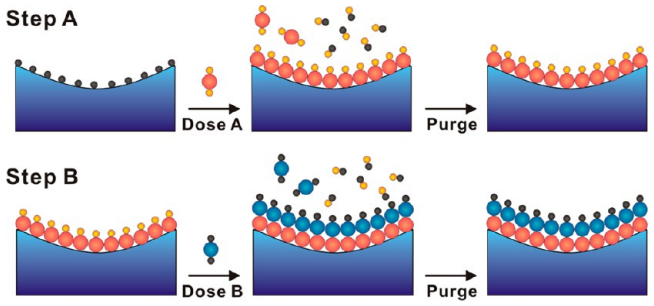

major cause of catalyst deactivation.[3−5] Encapsulation of metal nanoparticles, by various types of porous layers using techniques such as chemical vapor deposition (CVD) and sol−gel chemistry to form core−shell structures, shows good sintering resistance up to 800 °C.[6−11] However, in most cases there is a large decrease in catalytic activity due to mass transfer resistance associated with the protective shell (usually tens of nanometers thick). A method which allows atomically precise control over the thickness and composition of protective layers can preserve catalytic activity to the greatest extent while improving the stability.

Atomic layer deposition (ALD) is a thin film growth technique similar to CVD, except that the deposition is broken down into cycles each of which is a sequence of two surface reactions.[12−14] As shown in Scheme 1, ALD is carried out by first exposing the support to precursor A. The first step is a surface reaction between precursor A and functional groups on the support. The reaction stops when all available surface functional groups are consumed. Unreacted precursor and any volatile byproducts are then removed by inert gas purging. Following the purge, precursor B is introduced to the support to conduct the second surface reaction. A new surface with the same functional groups as the starting surface is generated after removing unreacted precursor and byproducts through a second inert gas purge. Because each surface reaction step is self-limiting, the amount of material deposited can be controlled precisely by selecting the number of ALD cycles. This makes it possible to achieve highly conformal thin films on substrates regardless of whether the surfaces are flat or possess high aspect ratio features, high surface area, or high porosity where CVD fails.[15−18] As a consequence, ALD has attracted great attention in a variety of applications such as electronics,[14,18] catalysis,[19−26] photovoltaics,[18,27,28] batteries,[29] and fuel cells.[23,30] In this Account, we discuss the application of ALD to heterogeneous catalysis. We will focus on strategies for synthesizing and stabilizing supported metal catalysts. The performance of the resulting catalysts will be also discussed.

2. ALD Strategies for Supported Metal Catalyst Synthesis

In many heterogeneous and electrocatalytic reactions, particle size plays a major role in catalyst performance.[1,31−33] Therefore, a synthesis method which can precisely tune the size of noble metal nanoparticles while maintaining a narrow size distribution can improve the catalytic performance. In addition, bimetallic catalysts offer the possibility to combine the advantages of each component and allow tuning of catalytic properties via nanoparticle composition and structure. While the design and economical synthesis of catalysts at the atomic scale represent a scientific grand challenge,[1] ALD offers a potential solution to this challenge. Both the size and composition of metal nanoparticles can be controlled precisely using ALD methods, and the ability to coat large areas using vapor phase infiltration has the potential for commercial viability. In the following sections, we will describe several implementations for the ALD synthesis of metal nanoparticles in order of increasing complexity.

2.1. A-Type ALD. The simplest implementation of ALD for synthesizing noble metal nanoparticles is to expose a solid support to a volatile metal precursor. At temperatures sufficiently low to prevent thermal decomposition, the precursor will chemisorb to a saturation coverage and retain a portion of its ligands. Metal nanoparticles form through aggregation after sequential heat treatments in oxidizing and reducing environments to remove the ligands. This is essentially a chemical grafting process, and has a very long history in the ALD literature.[34] However, high calcination temperatures can lead to particle sintering, and the need to cycle the temperature for different reactions is inconvenient.

2.2. AB-Type ALD. The next implementation is the "AB" method described in the Introduction. First, a volatile metal precursor A is exposed to a support until saturation. After purging the unreacted metal precursor A and byproducts, the surface is exposed to an oxidizing or reducing precursor B to form nanoparticles, remove remaining ligands, and create new active sites for the next cycle. Compared to the "A-type" ALD, the "AB" method can be performed over multiple cycles at a constant temperature lower than typical calcining temperatures so as to limit sintering. In this method, the particle size and loading can be controlled via the number of ALD cycles. As an example, Pt ALD uses

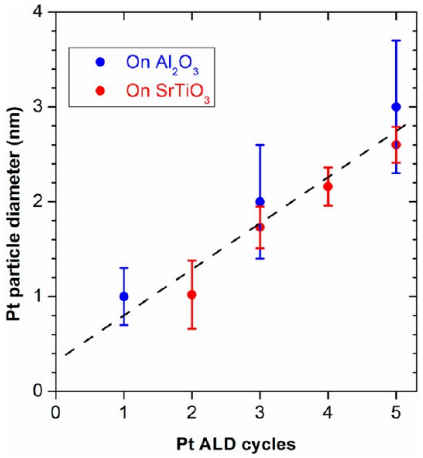

FIGURE 1. ALD Pt nanoparticle diameter versus number of Pt ALD cycles deposited on Al_2O_3 nanospheres and measured using TEM (blue symbols), and deposited on $SrTiO_3$ nanocubes and measured using X-ray diffraction (red symbols).

(methylcyclopentadienyl)trimethylplatinum ($MeCpPtMe_3$) and oxygen at 300 °C in two surface reactions:[35]

$$\text{A)}\ 3\,|\text{O}^* + 2\,\text{MeCpPtMe}_3\,(g) \rightarrow 2\,|\text{MeCpPtMe}_2^* + \text{CH}_4\,(g) + \text{CO}_2\,(g) + \text{H}_2\text{O}\,(g)$$

$$\text{B)}\ 2\,|\text{MeCpPtMe}_2^* + 24\,\text{O}_2\,(g) \rightarrow 2\,|\text{Pt}^* + 3\,|\text{O}^* + 16\,\text{CO}_2\,(g) + 13\,\text{H}_2\text{O}\,(g)$$

Figure 1 shows the diameter of ALD Pt nanoparticles versus the number of Pt ALD cycles. The blue symbols were determined from TEM analysis of ALD Pt nanoparticles deposited on spherical Al_2O_3. The red symbols were deduced using the Scherrer equation from X-ray diffraction measurements of ALD Pt nanoparticles deposited on $SrTiO_3$ nanocubes.[36] Figure 1 illustrates that the nanoparticle size is directly proportional to the number of ALD cycles and can be controlled with a precision of ~0.5 nm. The particle size is not strongly influenced by the substrate as evidenced by the similarity between depositions on the Al_2O_3 and $SrTiO_3$ surfaces. Similarly, for Pd the size of nanoparticles on an Al_2O_3 support was found to vary linearly between 1.1 (±0.5) nm and 2.9 (±0.9) nm as the number of Pd ALD cycles was increased from 1 to 25 using palladium(II) hexafluoroacetylacetonate [$Pd(hfac)_2$] and HCHO at 200 °C.[37]

Treating the support surface before ALD processing provides another means to control the particle size and loading. Since surface hydroxyl groups are typically the species responsible for metal precursor chemisorption, decreasing the surface hydroxyl density should reduce the metal loading. In agreement with this idea, when the hydroxyl density on an ALD Al_2O_3 surface, prior to Pd deposition, was reduced through thermal treatment, reaction with alcohols to form surface alkoxides, or reaction with trimethylaluminium (TMA), the Pd loading decreased.[38] For example, when an ethanol exposure was used to remove a fraction of the Al_2O_3 surface hydroxyls by conversion to ethoxide species prior to a $Pd(hfac)_2$ exposure, the Pd loading dropped by 36%, but the Pd particle size was unchanged.

SCHEME 2. Schematic Model of ABC-Type ALD[a]

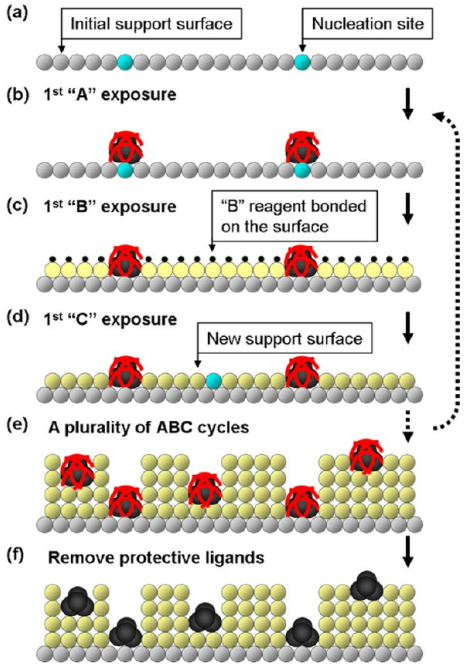

[a](a) An initial support with nucleation sites. (b) A volatile metal precursor A is introduced to the surface to form metal nanoparticles with part of ligands retained (red curves). Reagents B and C are then introduced to the surface sequentially to form a new support surface (c) and (d). (e) New support and metal nanoparticles protected by ligands are formed on the initial support surface after a plurality of ABC cycles. (f) The protective ligands are removed to activate metal nanoparticles. Reprinted with permission from ref 39.

Temperature can also influence particle size in ALD. In situ quartz crystal microbalance (QCM) measurements demonstrated that $Pd(hfac)_2$ chemisorption on oxide surfaces can occur at temperatures as low as 80 °C, far below the minimum temperature of 200 °C required to strip off the remaining hfac ligands using HCOH.[37,39] This finding suggested that a route to smaller Pd nanoparticles involves chemisorption of $Pd(hfac)_2$ at lower temperatures to reduce agglomeration. Indeed, low-temperature deposition of $Pd(hfac)_2$ yielded a particle size of only 0.8 ± 0.2 nm and a significantly narrower particle size distribution compared to the standard 200 °C $Pd(hfac)_2$ adsorption.[38]

2.3. ABC-Type ALD. Given that higher temperatures can induce sintering through agglomeration, another ALD process variation, low temperature "ABC-type" ALD, has been developed as depicted in Scheme 2.[37,39] This procedure combines the deposition of catalytic metal at low temperature (50−80 °C), the A-reaction, with deposition of new support material, the B- and C-reactions. Here the newly

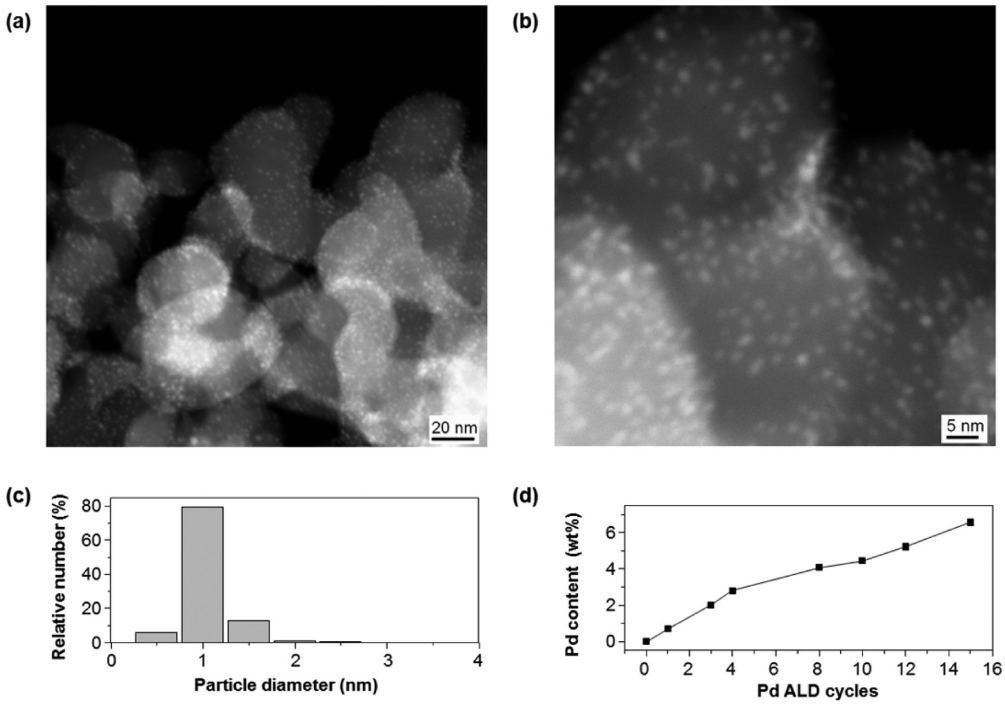

FIGURE 2. Morphology, size distribution histogram, and weight percentage of as-prepared Pd nanoparticles on 10-cycle Al_2O_3 coated silica gel support by different cycles of ABC-type Pd ALD at 80 °C: STEM images of an as-prepared 15 cycles of ABC-type Pd ALD sample at low (a) and high (b) magnifications. (c) Size distribution histogram of Pd nanoparticles. (d) Pd content by weight percentage for different Pd ALD cycles. Reprinted with permission from ref 39.

created support not only provides additional nucleation sites for metal deposition (Scheme 2c–e) but also inhibits agglomeration during the activation step (Scheme 2f). Highly uniform, 1 nm Pd nanoparticles with a wide range of loadings were successfully synthesized using the A/B/C sequence: $Pd(hfac)_2/TMA/H_2O$ at 80 °C (Figure 2). Treatment with formalin removes the capping hfac ligands (red curves in Scheme 2f), leaving the metal particles accessible for chemisorption and catalytic function. Diffuse reflectance infrared Fourier transform spectroscopy (DRIFTS) measurements of chemisorbed CO, performed after each step in the ABC process, support the capping, ligand removal, and accessibility of the metal particles depicted in Scheme 2. To date Pd,[37,39] Pt,[39] and Ag metal particles have been prepared on alumina and titania supports. The Pt/TiO_2 system yielded the smallest metal particles so far with an average particle size of 0.5 nm at a loading of 1.2 wt %. High resolution scanning transmission electron microscopy (STEM) images show Pt rafts with a large percentage of monomer and oligomer species.

2.4. ABCD-Type ALD. Supported bimetallic nanoparticle catalysts can be also synthesized with precise control over both the particle size and composition by simply combining two metal components. Here AB represents the ALD sequence for one component, and CD represents the second component. The size of the bimetallic particles can be controlled via the total number of ALD cycles. Moreover, the composition will be dictated by the relative number of ALD cycles used for each component. Finally, the structures of the bimetallic nanoparticles may be controlled by the order in which the individual cycles are executed. One of the appealing features of ALD for the atom scale synthesis of bimetallics is that once a procedure is developed to create the desired nanoparticles, the same process can be used to deposit them on virtually any substrate, and at any quantity.

2.4.1. ALD of Pt–Pd Nanoparticles. Pt–Pd, ~1 nm diameter mixed-metal nanoparticles were synthesized over ALD modified SiO_2 gel (SA 100 m^2/g) using $MeCpPtMe_3–O_2$ cycles for Pt ALD and $Pd(hfac)_2$–HCHO cycles for Pd ALD.[40] The composition of Pt–Pd nanoparticles could be adjusted in two ways. Due to the different kinetics for the ALD Pt and Pd reactions, the Pt metal loading and the resulting Pt–Pd composition could be varied by adjusting the deposition temperature while the Pd loading remained constant with temperature. Alternatively, the relative number of Pt and Pd ALD cycles can be used to tune the composition.

As an example, Pt–Pd mixed-metal nanoparticles exhibiting a mean size of 1.2 ± 0.4 nm by STEM and a 1:1 molar

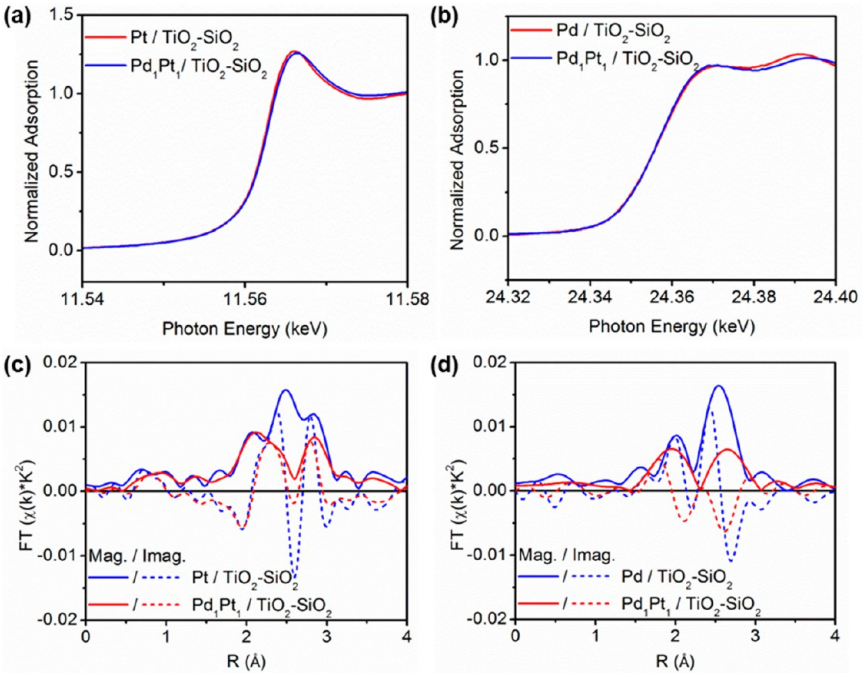

FIGURE 3. $Pd_1Pt_1/5c\,TiO_2/SiO_2$ XANES of (a) Pt edge and (b) Pd edge and Fourier transform of EXAFS of (c) Pt edge and (d) Pd edge in comparison to the monometallic nanoparticles. Reprinted with permission from ref 40. Copyright 2012 American Chemical Society.

ratio were synthesized using one Pt ALD cycle followed by one Pd ALD cycle.[40] The Pt–Pd nanoparticle structure was investigated using X-ray absorption spectroscopy (XAS) measurements at both the Pt L_3 edge (11.56 KeV) and the Pd K edge (24.35 KeV), shown in Figure 3. The as-prepared samples were reduced in H_2 at 250 °C for 1 h to obtain a fully metallic state prior to performing the XAS measurements. Small shifts in the edge position and changes in shape for both the Pt and Pd edges were clearly observed. Significant changes in the magnitude and imaginary part of both the Pt and Pd extended X-ray absorption fine structure (EXAFS) measurements indicated second scatters in the first shell structure, i.e. a bimetallic nanoparticle. Furthermore, EXAFS model fitting showed that Pt–Pd forms a Pt-core, Pd-shell structure, independent of the preparation temperature and ALD pulse sequence. Density functional theory (DFT) was used to calculate the lowest energy configuration for the Pt–Pd binary system. In vacuum, there was no clear preference for either a Pt- or Pd-rich surface. However, the Pd-rich surface was found to be more stable with one monolayer of hydrogen adsorbed, in good agreement with the EXAFS results.[40]

2.4.2. ALD of Pt–Ru Nanoparticles. Pt–Ru nanoparticles were synthesized using $MeCpPtMe_3$–O_2 cycles for Pt ALD and 2,4-(dimethylpentadienyl)(ethylcyclopentadienyl) ruthenium(II) (Ru(DER))–O_2 cycles for Ru ALD at 300 °C.[22] Preliminary QCM measurements revealed that the growth rates of Pt and Ru during the Pt–Ru mixed-metal ALD were in close agreement with the growth rates of the individual components. Nanoparticles synthesized using 2c Ru ALD, 1c Pt ALD, and 1c Ru ALD on spherical Al_2O_3 yielded an average particle size of 1.2 ± 0.3 nm. XAS measurements at the Ru K-edge (22.12 KeV) showed a shift by ~3 eV to higher energy compared to a Ru/SiO_2 standard, suggesting the formation of bimetallic Pt–Ru. The magnitude of the Fourier transform clearly showed features consistent with Pt atoms in the first coordination shell of Ru. Ru K-edge fitting yielded coordination numbers of 3.8 for Ru–Ru and 4.5 for Ru–Pt. In addition, the Ru–Pt nanoparticles supported on spherical Al_2O_3 powder exhibited a much higher reactivity in the methanol decomposition reaction compared to a physical mixture of Ru and Pt monometallic catalysts. While these experiments confirm the formation of bimetallic nanoparticles, additional structural details (core–shell versus alloy) will require XAS data at the Pt K-edge.

3. Metal Oxide Overcoating on Metal Catalysts by ALD: Stabilization and Catalytic Performance

ALD metal oxide coatings, where a conformal and uniform metal oxide layer forms on metal nanoparticles as well as the support, have been studied as a method to stabilize the particle size.[20,21,25,41,42] These studies were motivated by the atomically precise control of layer thickness and

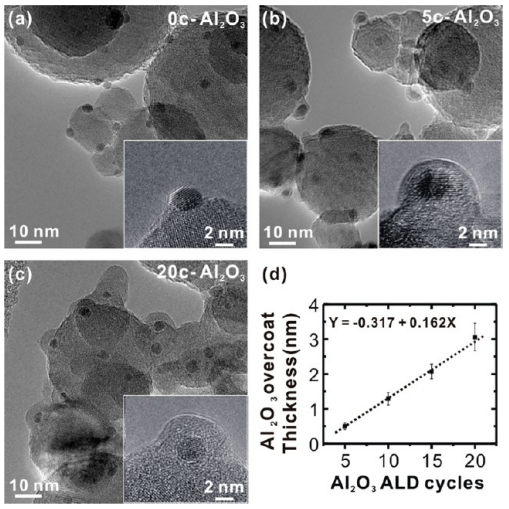

FIGURE 4. TEM images of Pd/Al_2O_3 catalysts on spherical alumina support following different numbers of ALD Al_2O_3 overcoating cycles (insets show higher magnification images). (a) Without overcoating; (b) 5 cycles Al_2O_3; (c) 20 cycles Al_2O_3; (d) thickness of Al_2O_3 overcoats versus ALD cycles. Reprinted with permission from ref 43. Copyright 2012 American Chemical Society.

composition afforded by ALD in comparison with other methods such as chemical vapor deposition and sol–gel chemistry.[6–11] For example, we recently showed that ALD Al_2O_3 layers could be precisely deposited on Pd nanoparticle catalysts at a growth rate of ~1.6 Å/cycle (Figure 4).[43] The ability to form ultrathin coatings has the potential to minimize the mass transfer resistance problem. In this section, we discuss the stability, accessibility, and catalytic performance of ALD alumina-overcoated Pd/Al_2O_3 catalysts.

3.1. Stabilization. One may anticipate that the overcoat thickness would be critical to catalyst performance. If the coating is too thick, it will reduce the catalytic activity, but if it is too thin sintering will not be inhibited. A recent study of methanol decomposition on uncoated and alumina-coated Pd nanoparticles demonstrates the effect of "overcoating" on both particle stability and activity.[21] Surprisingly, a single ALD Al_2O_3 cycle (~0.1 nm) was sufficient to suppress sintering of Pd nanoparticles during methanol decomposition at 270 °C for 6 h. Uncoated Pd particles doubled in size after the same treatment. Figure 5a displays the methanol conversion measured at 270 °C for Pd catalysts with 0–32 cycles of ALD Al_2O_3 overcoat. For 1–16 overcoat cycles, the catalytic activity was essentially identical. In fact, the catalysts prepared with overcoats in this range showed slightly higher activities than the uncoated catalysts, consistent with loss of surface area by the unprotected Pd via sintering. Beyond 16 overcoat cycles, the catalytic activity decreased.

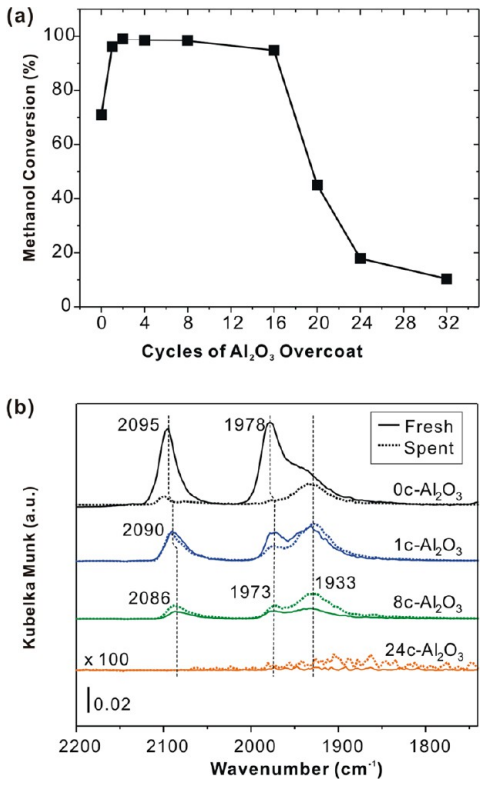

FIGURE 5. (a) Methanol conversion for Pd catalysts with 0–32 cycles of ALD Al_2O_3 overcoating in the methanol decomposition reaction carried out at 270 °C. (b) DRIFTS spectra of CO chemisorbed to saturation coverage on fresh and used Pd catalysts with different numbers of ALD Al_2O_3 overcoat cycles (0c-, 1c-, 8c-, and 24c-Al_2O_3). Spectra for the used 24c-Al_2O_3 samples were enlarged by ×100. Reprinted with permission from ref 21.

At 24 cycles, the catalyst had lost nearly 80% of its activity, and 32 cycles effectively shut off all conversion.

DRIFTS of CO chemisorbed on these materials revealed that the first few ALD Al_2O_3 cycles nucleate preferentially at Pd edge and corner sites as seen by the loss of bridged and linear CO peaks at 1978 and 2095 cm^{-1}, respectively (Figure 5b).[21] Since the Pd atoms on the low-coordination sites contribute little to the dehydrogenation reaction pathway for methanol decomposition,[44] the catalytic activity was not affected by the ALD Al_2O_3 overcoats. With increasing numbers of ALD Al_2O_3 overcoating cycles, the Al_2O_3 deposit begins to intrude on the Pd(111) sites and eventually leads to the complete particle encapsulation and no detectable CO chemisorption on the 24c-Al_2O_3 overcoated Pd sample (Figure 5b).

3.2. Porosity Generation within ALD Overcoats. For overcoated catalysts, it is crucial to maintain the access of reagents to the embedded metal nanoparticles. In the case of oxide overcoats prepared by sol–gel chemistry, there have been mainly two ways to generate pores within the

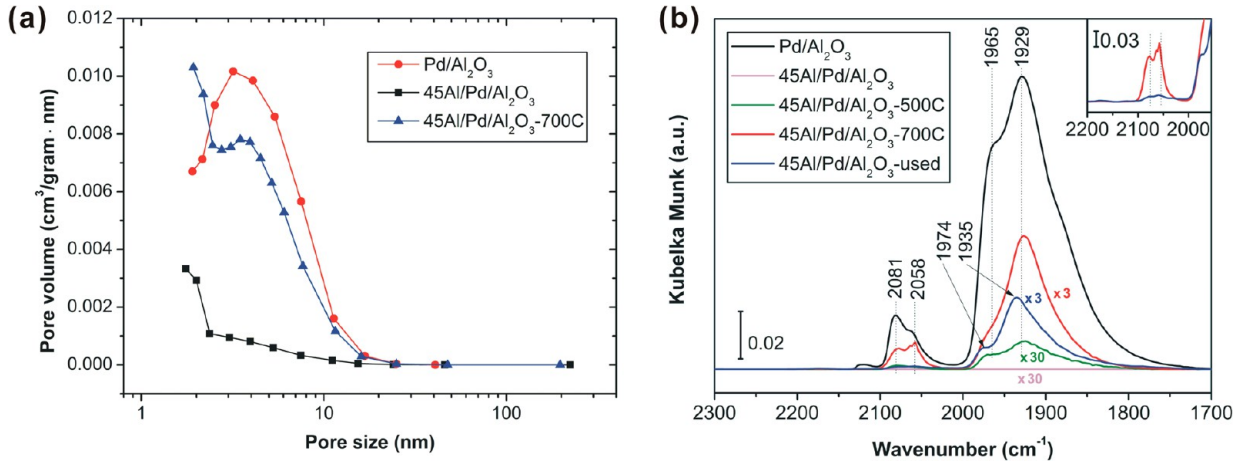

FIGURE 6. Structural characterization of ALD Al_2O_3 overcoats and accessibility of embedded Pd NPs after high temperature treatments. (a) Pore size distribution on the uncoated Pd/Al_2O_3, as-coated $45Al/Pd/Al_2O_3$, and $45Al/Pd/Al_2O_3$-700C samples. (b) IR spectra of CO chemisorption on the Pd samples with and without ALD Al_2O_3 overcoats at the CO saturation coverage: the uncoated Pd/Al_2O_3, fresh $45Al/Pd/Al_2O_3$, $45Al/Pd/Al_2O_3$-500C, $45Al/Pd/Al_2O_3$-700C, and $45Al/Pd/Al_2O_3$-used samples. Inset is the higher wavenumber region for the $45Al/Pd/Al_2O_3$-700C and $45Al/Pd/Al_2O_3$-used samples showing the near absence of edge and corner sites after reaction. Reprinted with permission from ref 20.

oxide overlayer: (i) sol–gel method combined with organic growth-directing agents, such as dendrimers, where the pores are formed by removal of the organic molecules through calcination;[7,8] and (ii) a surface-protected etching procedure.[11] For ALD protective overcoats, a number of methods have been developed to generate and control porosity:

(i) *Self-inhibited growth*. By combining in situ QCM measurements, in situ quadrupole mass spectroscopy (QMS) with DFT calculations, we discovered that the as-deposited ALD Al_2O_3 overlayer on Pd nanoparticles is porous due to a self-poisoning, self-cleaning growth process.[43] CH_3* surface species, formed through dissociative chemisorption of TMA on Pd surfaces, behave as a poison to inhibit Al_2O_3 growth during subsequent ALD cycles. Indeed, in the first ~7 cycles of ALD Al_2O_3 on Pd surfaces, the observation of hydrogen by QMS[43] along with the detection of bare Pd sites through CO chemisorption measurements[21] indicated that the Al_2O_3 layer was porous. Methanol decomposition activity on the overcoated Pd catalysts also supports this conclusion.[21]

(ii) *High temperature treatment*. When the Al_2O_3 overcoat becomes thicker than ~2 nm, the embedded Pd nanoparticles are completely encapsulated as evidenced by the absence of CO chemisorption.[21] However, we found that pores could be generated through high temperature dehydration,[20,45] the removal of ALD-derived carbon residues, and dewetting of Al_2O_3 from the nanoparticle.[20] For example, an ~8 nm thick ALD Al_2O_3 overcoat of Pd/Al_2O_3 (45 cycles) became porous after calcination at 700 °C for 2 h in 10% oxygen in helium ($45Al/Pd/Al_2O_3$-700C).[20] As shown in Figure 6a, new pores, ~2 nm diameter, were generated on $45Al/Pd/Al_2O_3$-700C. DRIFTS of CO chemisorbed on the coated Pd/Al_2O_3 catalyst indicated the gradual restoration of nanoparticle accessibility after increasing treatment temperatures (Figure 6b). An interesting phenomenon was observed after subjecting the Al_2O_3 overcoated Pd sample to oxidative dehydrogenation of ethane (ODHE) at 675 °C for 28 h ($45Al/Pd/Al_2O_3$-used). By comparison to the uncoated Pd NPs, the features associated with CO bound to edges (linear CO and bridged CO at 2058 and 1965 cm^{-1}, respectively) and corners (linear CO at 2081 cm^{-1}) on the used samples had substantially lower intensities relative to the feature due to CO on facet planes (bridged CO at 1929 cm^{-1}), indicating that the Al_2O_3 preferentially decorated the low coordinated Pd sites as a result of the temperature-induced structural changes.

(iii) *Organic porogens*. Liang et al. recently showed that highly porous Al_2O_3 films were formed on Pt nanoparticles by oxidizing aluminum alkoxide hybrid polymer films.[25] These films were deposited using alternating cycles of TMA and ethylene glycol for alucone molecular layer deposition (MLD) followed by calcination to remove the organic component. Hydrogen chemisorption analysis showed that the Pt dispersion only decreased from 65% to 38% after applying 40 cycles of alucone MLD followed by

calcination, verifying the high porosity of the Al_2O_3 film.

(iv) *Selective growth*. In this method, organic molecules are attached to the metal nanoparticle prior to the ALD overcoating treatment. The role of these organic molecules is to mask the nanoparticles and prevent growth of the oxide overcoat on the metal surface in a manner similar to the aforementioned ABC-type ALD.[39] After removing the organic molecules by oxidation, the metal nanoparticle will be surrounded by a metal oxide "nanobowl" where the size of the bowl can be controlled by selecting the appropriate masking agent and controlling the number of overcoat cycles.[46]

3.3. Catalytic Performance. An interesting and potentially important situation arises when the low coordination metal sites exhibit undesirable catalytic properties. In this case, preferential blocking of these undesirable sites by oxide overcoats could produce a more selective catalytic material. For instance, in methanol decomposition, the undesired carbon−oxygen bond breakage reaction pathway to carbon deposition preferentially occurs at the low coordination Pd sites, while the desired dehydrogenation reaction pathway takes place at Pd(111) terrace sites.[44] Therefore, the catalytic activity ehancement along with the improved stability of Pd nanoparticles was achieved on the alumina overcoated Pd catalysts for methanol decomposition since the ALD Al_2O_3 preferentially decorated the low coordination Pd sites.[21]

A second example of this potential can be seen in the comparison between ALD Al_2O_3 coated and uncoated Pd/Al_2O_3 catalysts for the ODHE reaction.[20] Supported Pd nanoparticles are notorious for deactivation by coke formation during alkane dehydrogenation.[47] In our hands a conventional Pd/Al_2O_3 catalyst completely deactivated in less than 30 min during the ODHE reaction. Post-mortem examination of the materials revealed carbon fibers to such an extent that the reactor was completely plugged, and the Pd had sintered extensively. In contrast, Al_2O_3 overcoated Pd nanoparticles exhibited excellent size stability and resistance to coke formation over 2 days of reaction testing at 675 °C and produced near-equilibrium yields of the desired ethylene product. In this study, we discovered that the edge and corner atoms played a central role for sintering, coking, and undesired reactions from C−C bond breaking.[48] Therefore, exceptional resistance to sintering and coking in high temperature catalytic reactions, along with significant selectivity enhancement, was achieved because the edge and corner atoms were selectively blocked and stabilized by alumina overcoats.

In the aforementioned examples, the improved catalytic selectivity was an unanticipated consequence of the selective Al_2O_3 deposition on particular Pd sites. However, the *"selective growth"* approach described above for catalyst stabilization offers the potential for much greater control and flexibility over the catalytic selectivity through judicious selection of appropriate molecular templating agents to fashion the "nanobowl". In analogy with the well-known selective catalysis achieved through micropore size and shape in zeolite and enzyme catalysts, it is conceivable that precise control over the pore size and pore shape within metal oxide overcoats could give rise to shape-selective catalytic function.

4. Conclusions and Prospects

In this Account, we illustrated the synthesis and stabilization of supported metal catalysts by ALD, taking advantage of its self-limiting character. The precise control over metal particle size, composition, and structure is achieved along with great flexibility by the combination of ALD sequence, surface treatment, and deposition temperature. Similarly, stabilization of metal particles by applying ALD oxide overcoats demonstrated important advantages from atomically precise control of protective layer thickness and composition compared to conventional methods such as CVD and sol−gel chemistry. Specifically, selective blocking of low coordination metal atoms by oxide overcoats provides a new strategy for enhancing both the durability and selectivity of metal catalysts. Moreover, the potential to control pore size and shape within an ALD oxide overcoat could provide shape-selective catalytic function.

ALD has been successfully commercialized in the microelectronics industry. While there are technical and financial challenges to transitioning ALD from the research laboratory into the catalyst industry, they are not insurmountable. The main technical challenge is scaling up the process to the quantity of material relevant to catalyst manufacturing. Fixed-bed and/or fluidized-bed reactors more suited for coating high-surface-area powders or monoliths would be employed rather than equipment designed to coat silicon wafers. Successful examples of these designs have been reported in the literature.[25,34] Whether the catalyst manufacturer can justify the capital and production costs associated with ALD will depend on the value of the end product.

The work at Argonne National Laboratory was supported by the Office of Basic Energy Sciences, Division of Chemical Sciences, Geosciences, and Biosciences, U.S. Department of Energy, under the Hydrogen Fuel Initiative (initial metal particle synthesis, low temperature overcoating methanol decomposition, overcoat pore generation) and the Institute for Atom-efficient Chemical Transformations (IACT), an Energy Frontier Research Center, funded by the U.S. Department of Energy, Office of Basic Energy Sciences (alloy particle synthesis and overcoat chemical mechanism). The work at Northwestern University was financially supported by The Dow Chemical Company under the Dow Methane Challenge Award (ethane oxidative dehydrogenation and inhibition of coke formation).

BIOGRAPHICAL INFORMATION

Junling Lu received his B.S. in physics from Henan University in 1998 and Ph.D. from Institute of Physics, Chinese Academy of Sciences in 2007. After graduation, he spent 3 years in Prof. Peter C. Stair's group as a postdoctoral fellow at Northwestern University, focusing on design and synthesis of advanced catalysts with ALD. He has been working in Dr. Jeffrey W. Elam's group as a postdoctoral fellow at Argonne National Laboratory since 2010, continuing the research in the application of ALD in catalysis.

Jeffrey W. Elam received his B.S. in chemistry from Cornell University in 1988 and Ph.D. from University of Chicago in 1995. Currently, he is a principal chemist at Argonne National Laboratory. He won two R&D 100 awards for research in ultrananocrystalline diamond mechanical seals in 2008 and for his development of large area microchannel plates in 2012.

Peter C. Stair received his B.S. in chemistry from Stanford University in 1972 and Ph.D. from University of California, Berkeley in 1977. Currently, he is Professor of Chemistry at Northwestern University and Senior Scientist in the Chemical Sciences and Engineering Division at Argonne National Laboratory. He is a past recipient of the Alexander von Humboldt Senior Scientist Award and recipient of the 2010 ACS George Olah Award in Hydrocarbon or Petroleum Chemistry.

FOOTNOTES

*To whom correspondence should be addressed. E-mail: pstair@northwestern.edu.
The authors declare no competing financial interest.

REFERENCES

1 Cuenya, B. R. Synthesis and catalytic properties of metal nanoparticles: Size, shape, support, composition, and oxidation state effects. *Thin Solid Films* **2010**, *518*, 3127–3150.
2 Gates, B. C. Supported Metal-Clusters - Synthesis, Structure, and Catalysis. *Chem. Rev.* **1995**, *95*, 511–522.
3 Bartholomew, C. H. Mechanisms of catalyst deactivation. *Appl. Catal. A* **2001**, *212*, 17–60.
4 Wanke, S. E.; Flynn, P. C. Sintering of Supported Metal-Catalysts. *Catal. Rev.* **1975**, *12*, 92–135.
5 Campbell, C. T.; Parker, S. C.; Starr, D. E. The effect of size-dependent nanoparticle energetics on catalyst sintering. *Science* **2002**, *298*, 811–814.
6 Seipenbusch, M.; Binder, A. Structural Stabilization of Metal Nanoparticles by Chemical Vapor Deposition-Applied Silica Coatings. *J. Phys. Chem. C* **2009**, *113*, 20606–20610.
7 Ott, L. S.; Finke, R. G. Transition-metal nanocluster stabilization for catalysis: A critical review of ranking methods and putative stabilizers. *Coord. Chem. Rev.* **2007**, *251*, 1075–1100.
8 Joo, S. H.; Park, J. Y.; Tsung, C. K.; Yamada, Y.; Yang, P. D.; Somorjai, G. A. Thermally stable Pt/mesoporous sililca core-shell nanocatalysts for high-temperature reactions. *Nat. Mater.* **2009**, *8*, 126–131.
9 Park, J. N.; Forman, A. J.; Tang, W.; Cheng, J. H.; Hu, Y. S.; Lin, H. F.; McFarland, E. W. Highly Active and Sinter-Resistant Pd-Nanoparticle Catalysts Encapsulated in Silica. *Small* **2008**, *4*, 1694–1697.
10 Arnal, P. M.; Comotti, M.; Schuth, F. High-temperature-stable catalysts by hollow sphere encapsulation. *Angew. Chem., Int. Ed.* **2006**, *45*, 8224–8227.
11 Zhang, Q.; Lee, I.; Ge, J. P.; Zaera, F.; Yin, Y. D. Surface-Protected Etching of Mesoporous Oxide Shells for the Stabilization of Metal Nanocatalysts. *Adv. Funct. Mater.* **2010**, *20*, 2201–2214.
12 George, S. M. Atomic Layer Deposition: An Overview. *Chem. Rev.* **2010**, *110*, 111–131.
13 Puurunen, R. L. Surface chemistry of atomic layer deposition: A case study for the trimethylaluminum/water process. *J. Appl. Phys.* **2005**, *97*, 121301.
14 Suntola, T.; Hyvarinen, J. Atomic Layer Epitaxy. *Annu. Rev. Mater. Sci.* **1985**, *15*, 177–195.
15 Elam, J. W. In *Atomic Layer Deposition of Nanostructured Materials*; Pinna, N., Knez, M., Eds.; Wiley-VCH: Weinheim, 2012.
16 Pagan-Torres, Y. J.; Gallo, J. M. R.; Wang, D.; Pham, H. N.; Libera, J. A.; Marshall, C. L.; Elam, J. W.; Datye, A. K.; Dumesic, J. A. Synthesis of Highly Ordered Hydrothermally Stable Mesoporous Niobia Catalysts by Atomic Layer Deposition. *ACS Catal.* **2011**, *1*, 1234–1245.
17 Lim, B. S.; Rahtu, A.; Gordon, R. G. Atomic layer deposition of transition metals. *Nat. Mater.* **2003**, *2*, 749–754.
18 Knez, M.; Niesch, K.; Niinisto, L. Synthesis and surface engineering of complex nanostructures by atomic layer deposition. *Adv. Mater.* **2007**, *19*, 3425–3438.
19 Lu, J. L.; Lei, Y.; Elam, J. W. In *Noble Metals*; Su, Y.-H. , Ed.; InTech: Rijeka, 2012; Vol. 8.
20 Lu, J. L.; Fu, B. S.; Kung, M. C.; Xiao, G. M.; Elam, J. W.; Kung, H. H.; Stair, P. C. Coking- and Sintering- Resistant Palladium Catalysts Achieved Through Atomic Layer Deposition. *Science* **2012**, *335*, 1205–1208.
21 Feng, H.; Lu, J. L.; Stair, P. C.; Elam, J. W. Alumina Over-coating on Pd Nanoparticle Catalysts by Atomic Layer Deposition: Enhanced Stability and Reactivity. *Catal. Lett.* **2011**, *141*, 512–517.
22 Christensen, S. T.; Feng, H.; Libera, J. L.; Guo, N.; Miller, J. T.; Stair, P. C.; Elam, J. W. Supported Ru-Pt Bimetallic Nanoparticle Catalysts Prepared by Atomic Layer Deposition. *Nano Lett.* **2010**, *10*, 3047–3051.
23 King, J. S.; Wittstock, A.; Biener, J.; Kucheyev, S. O.; Wang, Y. M.; Baumann, T. F.; Giri, S. K.; Hamza, A. V.; Baeumer, M.; Bent, S. F. Ultralow loading Pt nanocatalysts prepared by atomic layer deposition on carbon aerogels. *Nano Lett.* **2008**, *8*, 2405–2409.
24 Feng, H.; Elam, J. W.; Libera, J. A.; Pellin, M. J.; Stair, P. C. Oxidative dehydrogenation of cyclohexane over alumina-supported vanadium oxide nanoliths. *J. Catal.* **2010**, *269*, 421–431.
25 Liang, X. H.; Li, J. H.; Yu, M.; McMurray, C. N.; Falconer, J. L.; Weimer, A. W. Stabilization of Supported Metal Nanoparticles Using an Ultrathin Porous Shell. *ACS Catal.* **2011**, *1*, 1162–1165.
26 Stair, P. C. Synthesis of Supported Catalysts by Atomic Layer Deposition. *Top. Catal.* **2012**, *55*, 93–98.
27 Chen, Y. W.; Prange, J. D.; Duhnen, S.; Park, Y.; Gunji, M.; Chidsey, C. E. D.; McIntyre, P. C. Atomic layer-deposited tunnel oxide stabilizes silicon photoanodes for water oxidation. *Nat. Mater.* **2011**, *10*, 539–544.
28 Martinson, A. B. F.; Elam, J. W.; Pellin, M. J. Atomic layer deposition of Cu(2)S for future application in photovoltaics. *Appl. Phys. Lett.* **2009**, *94*, 123107.
29 Scott, I. D.; Jung, Y. S.; Cavanagh, A. S.; An, Y. F.; Dillon, A. C.; George, S. M.; Lee, S. H. Ultrathin Coatings on Nano-$LiCoO_2$ for Li-Ion Vehicular Applications. *Nano Lett.* **2011**, *11*, 414–418.
30 Chao, C. C.; Hsu, C. M.; Cui, Y.; Prinz, F. B. Improved Solid Oxide Fuel Cell Performance with Nanostructured Electrolytes. *ACS Nano* **2011**, *5*, 5692–5696.
31 Chen, M. S.; Goodman, D. W. Catalytically active gold: From nanoparticles to ultrathin films. *Acc. Chem. Res.* **2006**, *39*, 739–746.
32 Bell, A. T. The impact of nanoscience on heterogeneous catalysis. *Science* **2003**, *299*, 1688–1691.
33 Lei, Y.; Mehmood, F.; Lee, S.; Greeley, J.; Lee, B.; Seifert, S.; Winans, R. E.; Elam, J. W.; Meyer, R. J.; Redfern, P. C.; Teschner, D.; Schlogl, R.; Pellin, M. J.; Curtiss, L. A.; Vajda, S. Increased Silver Activity for Direct Propylene Epoxidation via Subnanometer Size Effects. *Science* **2010**, *328*, 224–228.

34 Haukka, S.; Lakomaa, E. L.; Suntola, T. Adsorption controlled preparation of heterogeneous catalysts. *Adsorption and Its Applications in Industry and Environmental Protection, Vol I: Applications in Industry, Studies in Surface Science and Catalysis Series,* **1999**, *120*, 715–750.

35 Kessels, W. M. M.; Knoops, H. C. M.; Dielissen, S. A. F.; Mackus, A. J. M.; van de Sanden, M. C. M. Surface reactions during atomic layer deposition of Pt derived from gas phase infrared spectroscopy. *Appl. Phys. Lett.* **2009**, *95*, 013114/1–013114/3.

36 Christensen, S. T.; Elam, J. W.; Rabuffetti, F. A.; Ma, Q.; Weigand, S. J.; Lee, B.; Seifert, S.; Stair, P. C.; Poeppelmeier, K. R.; Hersam, M. C.; Bedzyk, M. J. Controlled Growth of Platinum Nanoparticles on Strontium Titanate Nanocubes by Atomic Layer Deposition. *Small* **2009**, *5*, 750–757.

37 Lu, J.; Stair, P. C. Nano/Subnanometer Pd Nanoparticles on Oxide Supports Synthesized by AB-type and Low-Temperature ABC-type Atomic Layer Deposition: Growth and Morphology. *Langmuir* **2010**, *26*, 16486–16495.

38 Feng, H.; Elam, J. W.; Libera, J. A.; Stair, P. C.; Miller, J. T. Subnanometer Palladium Particles Synthesized by Atomic Layer Deposition. *ACS Catal.* **2011**, *1*, 665–673.

39 Lu, J. L.; Stair, P. C. Low-Temperature ABC-Type Atomic Layer Deposition: Synthesis of Highly Uniform Ultrafine Supported Metal Nanoparticles. *Angew. Chem., Int. Ed.* **2010**, *49*, 2547–2551.

40 Lei, Y.; Liu, B.; Lu, J. L.; Lobo, R.; Wu, T.; Feng, H.; Xia, X.; Mane, A. U.; Libera, J. A.; Greeley, J. P.; Miller, J. T.; Elam, J. W. Synthesis of Pt-Pd Core-Shell Nanostructures by Atomic Layer Deposition: Application in Propane Oxidative Dehydrogenation to Propylene. *Chem. Mater.* **2012**, *24*, 3525–3533.

41 Ma, Z.; Brown, S.; Howe, J. Y.; Overbury, S. H.; Dai, S. Surface modification of Au/TiO_2 catalysts by SiO_2 via atomic layer deposition. *J. Phys. Chem. C* **2008**, *112*, 9448–9457.

42 Zhang, X. Y.; Zhao, J.; Whitney, A. V.; Elam, J. W.; Van Duyne, R. P. Ultrastable substrates for surface-enhanced Raman spectroscopy: Al_2O_3 overlayers fabricated by atomic layer deposition yield improved anthrax biomarker detection. *J. Am. Chem. Soc.* **2006**, *128*, 10304–10309.

43 Lu, J. L.; Liu, B.; Greeley, J. P.; Feng, Z. X.; Libera, J. A.; Lei, Y.; Bedzyk, M. J.; Stair, P. C.; Elam, J. W. Porous Alumina Protective Coatings on Palladium Nanoparticles by Self-Poisoned Atomic Layer Deposition. *Chem. Mater.* **2012**, *24*, 2047–2055.

44 Schauermann, S.; Hoffmann, J.; Johanek, V.; Hartmann, J.; Libuda, J.; Freund, H. J. Catalytic activity and poisoning of specific sites on supported metal nanoparticles. *Angew. Chem., Int. Ed.* **2002**, *41*, 2532.

45 Ferguson, J. D.; Weimer, A. W.; George, S. M. Atomic layer deposition of ultrathin and conformal Al_2O_3 films on BN particles. *Thin Solid Films* **2000**, *371*, 95–104.

46 Ray, N. A.; Van Duyne, R. P.; Stair, P. C. Synthesis Strategy for Protected Metal Nanoparticles. *J. Phys. Chem. C* **2012**, *116*, 7748–7756.

47 Huff, M.; Schmidt, L. D. Ethylene Formation by Oxidative Dehydrogenation of Ethane over Monoliths at Very Short-Contact Times. *J. Phys. Chem.* **1993**, *97*, 11815–11822.

48 Helveg, S.; Lopez-Cartes, C.; Sehested, J.; Hansen, P. L.; Clausen, B. S.; Rostrup-Nielsen, J. R.; Abild-Pedersen, F.; Norskov, J. K. Atomic-scale imaging of carbon nanofibre growth. *Nature* **2004**, *427*, 426–429.